Multiscale wear modelling of cemented tungsten carbide tools in hard rock drilling

Dmitry Tkalich[★▲], Vladislav A. Yastrebov[★]
Alexandre Kane[•], Georges Cailletaud[★]

[★] *MINES ParisTech, Centre des Matériaux, CNRS UMR, Evry, France*

[▲] *National University of Singapore, Singapore*
[•] *Sintef, Trondheim, Norway*

Computational Modeling of Complex Materials Across the Scales
Paris, France
November 8, 2017

Outline

- Introduction
- Cemented tungsten carbide
- Microstructural model
- Mean-field model
- Tool-rock interaction
- Results
- Conclusion

Introduction

- Rotary percussive drilling
- Down-the-hole technique
- Gas / oil / geothermal energy

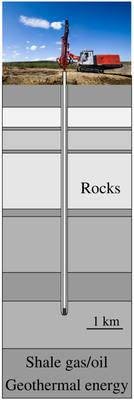

Used photo from Traxxon Ltd.

Introduction

- Rotary percussive drilling
- Down-the-hole technique
- Gas / oil / geothermal energy
- Cemented tungsten carbide (WC) inserts in a steel crown
- Impact and scratch of a hard rock
- Wear and failure of drilling tools

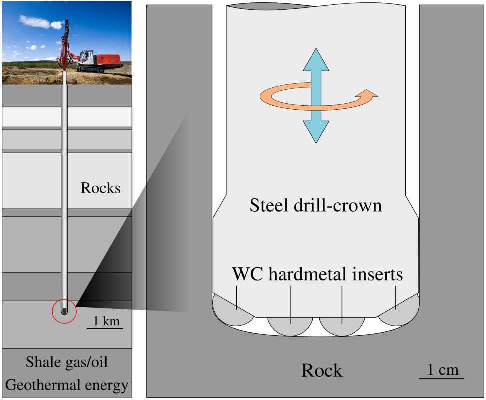

Used photo from Traxxon Ltd.

Introduction

- Rotary percussive drilling
- Down-the-hole technique
- Gas / oil / geothermal energy
- Cemented tungsten carbide (WC) inserts in a steel crown
- Impact and scratch of a hard rock
- Wear and failure of drilling tools

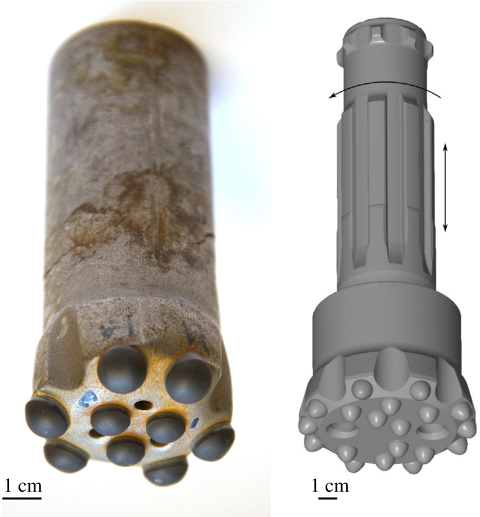

Drill-bit designs with spherical and ballistic-shape WC hardmetal inserts

Introduction

- Rotary percussive drilling
- Down-the-hole technique
- Gas / oil / geothermal energy
- Cemented tungsten carbide (WC) inserts in a steel crown
- Impact and scratch of a hard rock
- Wear and failure of drilling tools

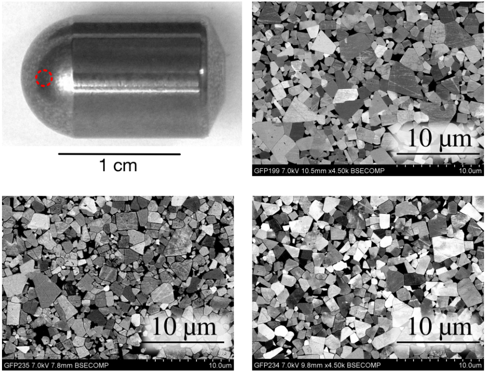

WC hardmetal insert and different microstructure

Introduction

- Rotary percussive drilling
- Down-the-hole technique
- Gas / oil / geothermal energy
- Cemented tungsten carbide (WC) inserts in a steel crown
- Impact and scratch of a hard rock
- Wear and failure of drilling tools

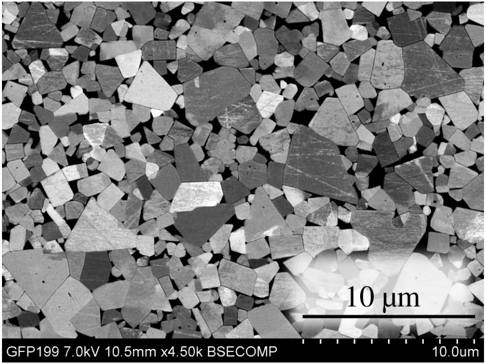

Microstructure

Introduction

- Rotary percussive drilling
- Down-the-hole technique
- Gas / oil / geothermal energy
- Cemented tungsten carbide (WC) inserts in a steel crown
- Impact and scratch of a hard rock
- Wear and failure of drilling tools

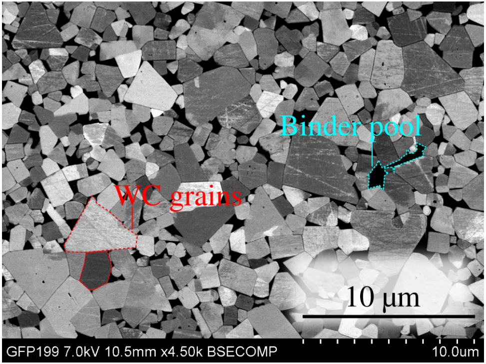

Microstructure
WC grains binded by binder (Co here)

Introduction

- Rotary percussive drilling
- Down-the-hole technique
- Gas / oil / geothermal energy
- Cemented tungsten carbide (WC) inserts in a steel crown
- Impact and scratch of a hard rock
- Wear and failure of drilling tools

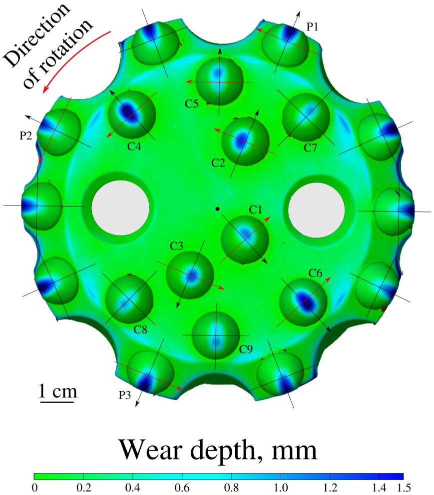

Wear pattern
(after 80 m drilled in hard rock)

Introduction

- Rotary percussive drilling
- Down-the-hole technique
- Gas / oil / geothermal energy
- Cemented tungsten carbide (WC) inserts in a steel crown
- Impact and scratch of a hard rock
- Wear and failure of drilling tools

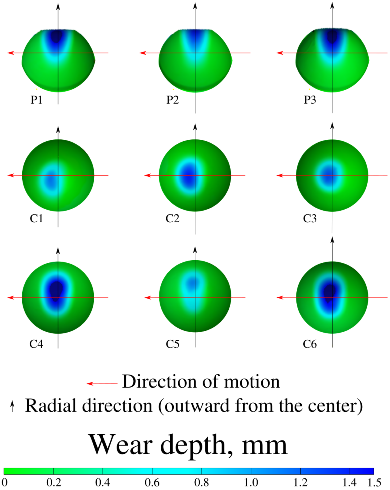

Wear pattern orientation
(after 80 m drilled in hard rock)

Introduction

- Rotary percussive drilling
- Down-the-hole technique
- Gas / oil / geothermal energy
- Cemented tungsten carbide (WC) inserts in a steel crown
- Impact and scratch of a hard rock
- Wear and failure of drilling tools

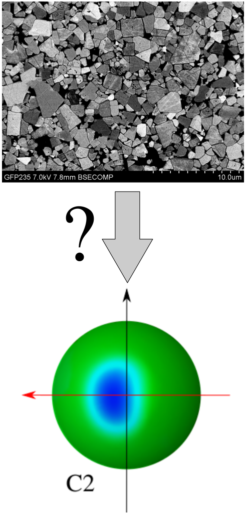

Objective: understand better the relationship between the wear resistance of WC hardmetals and its composition

Introduction

- Rotary percussive drilling
- Down-the-hole technique
- Gas / oil / geothermal energy
- Cemented tungsten carbide (WC) inserts in a steel crown
- Impact and scratch of a hard rock
- Wear and failure of drilling tools

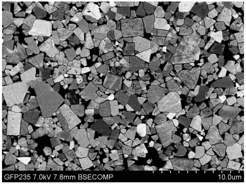

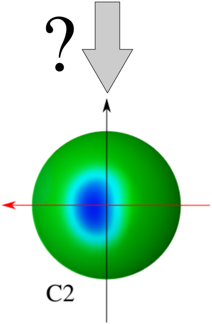

Objective: estimate *quantitatively* microstructural deformation mechanisms in WC hardmetals during hard rock drilling

Hard Metal

vs

Hard Rock

Topic

WC/Co

VS

KURU GRANITE

Material: cemented tungsten carbide

Main characteristics

- Brittle WC
- Ductile binder (Co, Ni, Fe)
- High hardness and wear resistance
- Very high melting point of WC prevents abrasive wear

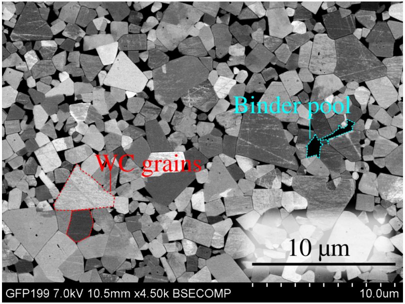

Microstructure
WC grains binded by binder (Co here)

Material: cemented tungsten carbide

Main characteristics

- Brittle WC
- Ductile binder (Co, Ni, Fe)
- High hardness and wear resistance
- Very high melting point of WC prevents abrasive wear

Microscopic mechanisms leading to macroscopic wear

- Fragmentation of WC grains
- Binder lost
- Tribofilm debonding with grains

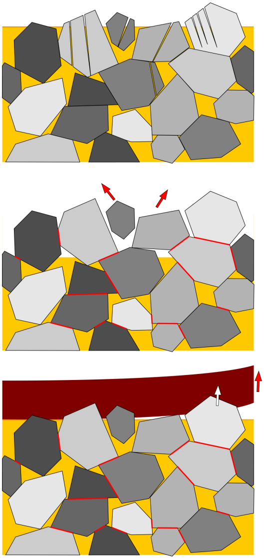

Wear mechanisms

Material: cemented tungsten carbide

Main characteristics

- Brittle WC
- Ductile binder (Co, Ni, Fe)
- High hardness and wear resistance
- Very high melting point of WC prevents abrasive wear

Microscopic mechanisms leading to macroscopic wear

- Fragmentation of WC grains
- Binder lost
- **Tribofilm** debonding with grains

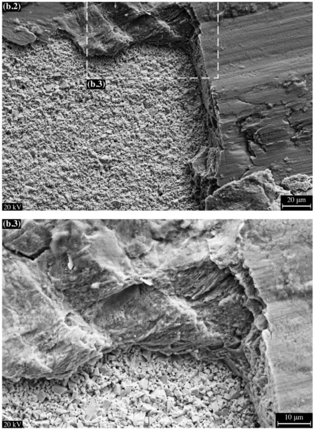

SEM showing a tribofilm formed after 80m drilling in hard rock[1]

[1] Tkalich et al, *Wear* 386-387 (2017)

Microstructural mechanical model: 2D

Physics

- Linear dimensions of the binder "quasi crystals" $\approx \; 10d_{\mathrm{WC}}$
- Cohesion WC/WC and WC/binder
- Anisotropic WC grains (hcp)

2D model

- Outlined SEM images converted to mesh microstructure
- Perfect interfaces
- Isotropic WC and binder
- Von Mises plasticity for the binder
- Non-associated pressure dependent plasticity for WC (Drucker-Prager)

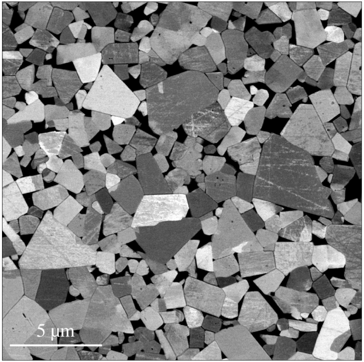

SEM image

[1] Tkalich, Cailletaud, Yastrebov, Kane, *Mech Mater* 105 (2017)

Microstructural mechanical model: 2D

Physics

- Linear dimensions of the binder "quasi crystals" $\approx\ 10d_{WC}$
- Cohesion WC/WC and WC/binder
- Anisotropic WC grains (hcp)

2D model

- Outlined SEM images converted to mesh microstructure
- Perfect interfaces
- Isotropic WC and binder
- Von Mises plasticity for the binder
- Non-associated pressure dependent plasticity for WC (Drucker-Prager)

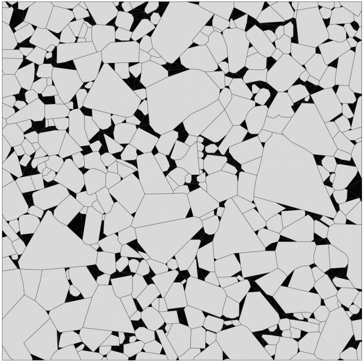

Outlined SEM image, CAD model

[1] Tkalich, Cailletaud, Yastrebov, Kane, *Mech Mater* 105 (2017)

Microstructural mechanical model: 2D

Physics

- Linear dimensions of the binder "quasi crystals" $\approx 10d_{WC}$
- Cohesion WC/WC and WC/binder
- Anisotropic WC grains (hcp)

2D model

- Outlined SEM images converted to mesh microstructure
- Perfect interfaces
- Isotropic WC and binder
- Von Mises plasticity for the binder
- Non-associated pressure dependent plasticity for WC (Drucker-Prager)

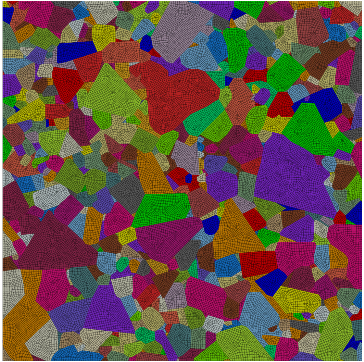

FE mesh

[1] Tkalich, Cailletaud, Yastrebov, Kane, *Mech Mater* 105 (2017)

Microstructural mechanical model: 2D

Physics

- Linear dimensions of the binder "quasi crystals" $\approx 10d_{WC}$
- Cohesion WC/WC and WC/binder
- Anisotropic WC grains (hcp)

2D model

- Outlined SEM images converted to mesh microstructure
- Perfect interfaces
- Isotropic WC and binder
- Von Mises plasticity for the binder
- Non-associated pressure dependent plasticity for WC (Drucker-Prager)

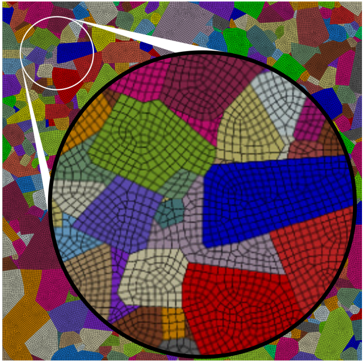

FE mesh

[1] Tkalich, Cailletaud, Yastrebov, Kane, *Mech Mater* 105 (2017)

Microstructural mechanical model: 2D results

Pure shear loading

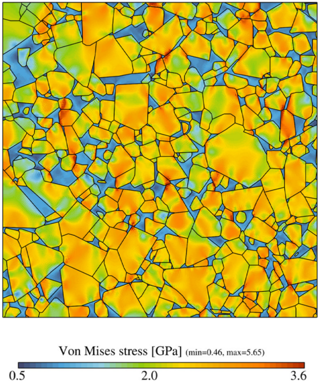

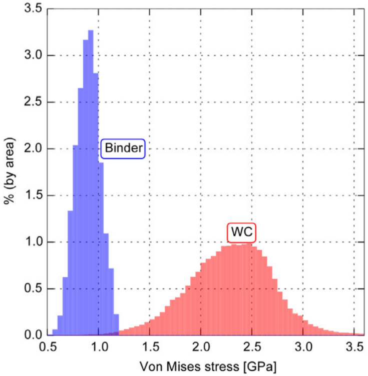

von Mises stress σ_{vM}

[1] Tkalich, Cailletaud, Yastrebov, Kane, *Mech Mater* 105 (2017)

Microstructural mechanical model: 2D results

Pure shear loading

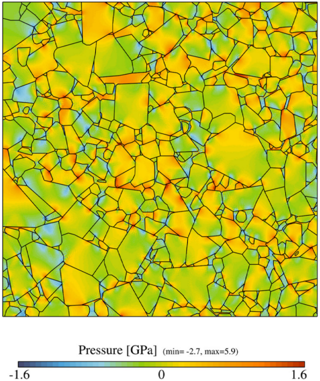

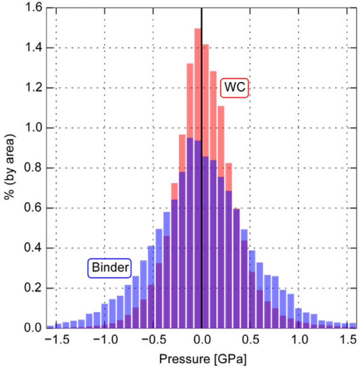

Pressure $P = -\mathrm{trace}(\underline{\sigma})/3$

[1] Tkalich, Cailletaud, Yastrebov, Kane, *Mech Mater* 105 (2017)

Microstructural mechanical model: 2D results

Pure shear loading

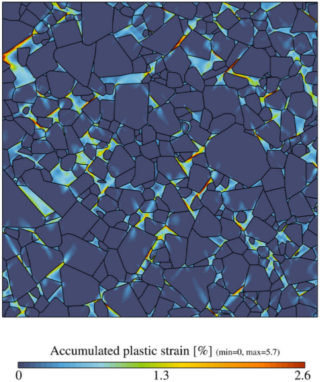

Accumulated plastic strain p

[1] Tkalich, Cailletaud, Yastrebov, Kane, *Mech Mater* 105 (2017)

Microstructural mechanical model: 2D results

Pure shear loading

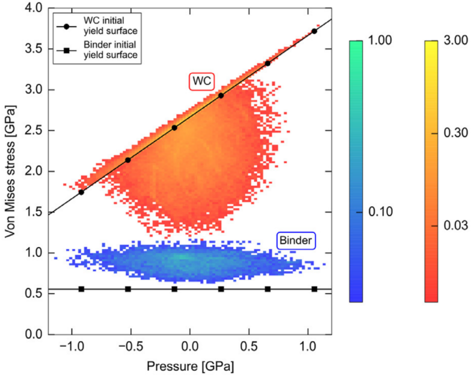

Joint probability density in von Mises – Pressure space $Pr(\sigma_{vM}, P)$

[1] Tkalich, Cailletaud, Yastrebov, Kane, *Mech Mater* 105 (2017)

It’s only 2D . . .

Microstructural mechanical model: 3D

Microstructural model

- Generate Voronoi tesselation (voro++[1])
- Every Voronoi grain is cut by randomly oriented planes[2]
- The smaller cut parts become the binder, the rest remains the WC
- Parameters:
  (1) number of cuts
  (2) binder volume fraction

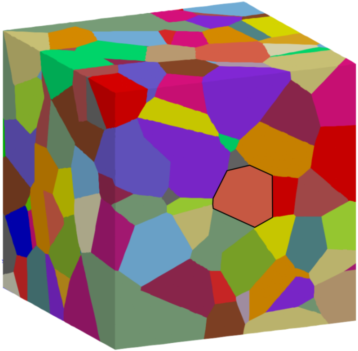

Voronoi grains

[1] Chris Rycroft `math.lbl.gov/voro++/`

[2] Tkalich, Yastrebov, Cailletaud, Kane, *Int J Solids Struct* 128 (2017)

Microstructural mechanical model: 3D

Microstructural model

- Generate Voronoi tesselation (voro++[1])
- Every Voronoi grain is cut by randomly oriented planes[2]
- The smaller cut parts become the binder, the rest remains the WC
- Parameters:
  (1) number of cuts
  (2) binder volume fraction

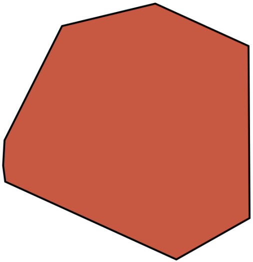

Example in 2D
Randomly oriented cuts

[1] Chris Rycroft `math.lbl.gov/voro++/`

[2] Tkalich, Yastrebov, Cailletaud, Kane, *Int J Solids Struct* 128 (2017)

Microstructural mechanical model: 3D

Microstructural model

- Generate Voronoi tesselation (voro++[1])
- Every Voronoi grain is cut by randomly oriented planes[2]
- The smaller cut parts become the binder, the rest remains the WC
- Parameters:
  (1) number of cuts
  (2) binder volume fraction

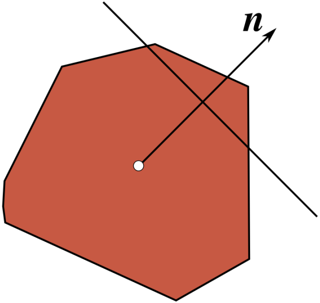

Example in 2D
Randomly oriented cuts

[1] Chris Rycroft `math.lbl.gov/voro++/`

[2] Tkalich, Yastrebov, Cailletaud, Kane, *Int J Solids Struct* 128 (2017)

Microstructural mechanical model: 3D

Microstructural model

- Generate Voronoi tesselation (voro++[1])
- Every Voronoi grain is cut by randomly oriented planes[2]
- The smaller cut parts become the binder, the rest remains the WC
- Parameters:
  (1) number of cuts
  (2) binder volume fraction

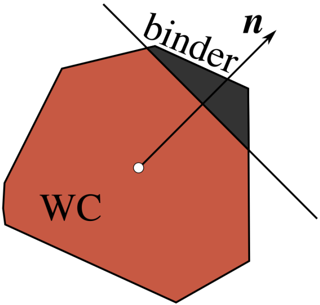

Example in 2D
Randomly oriented cuts

[1] Chris Rycroft math.lbl.gov/voro++/

[2] Tkalich, Yastrebov, Cailletaud, Kane, *Int J Solids Struct* 128 (2017)

Microstructural model

- Generate Voronoi tesselation (voro++[1])
- Every Voronoi grain is cut by randomly oriented planes[2]
- The smaller cut parts become the binder, the rest remains the WC
- Parameters:
  (1) number of cuts
  (2) binder volume fraction

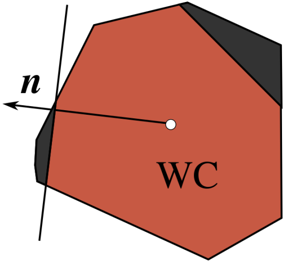

Example in 2D
Randomly oriented cuts

[1] Chris Rycroft `math.lbl.gov/voro++/`

[2] Tkalich, Yastrebov, Cailletaud, Kane, *Int J Solids Struct* 128 (2017)

Microstructural mechanical model: 3D

Microstructural model

- Generate Voronoi tesselation (voro++[1])
- Every Voronoi grain is cut by randomly oriented planes[2]
- The smaller cut parts become the binder, the rest remains the WC
- Parameters:
  (1) number of cuts
  (2) binder volume fraction

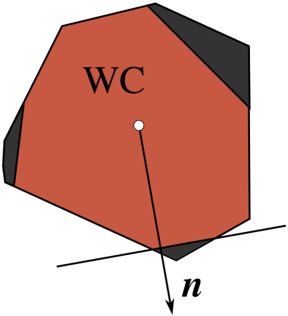

Example in 2D
Randomly oriented cuts

[1] Chris Rycroft `math.lbl.gov/voro++/`

[2] Tkalich, Yastrebov, Cailletaud, Kane, *Int J Solids Struct* 128 (2017)

Microstructural mechanical model: 3D

Microstructural model

- Generate Voronoi tesselation (voro++[1])
- Every Voronoi grain is cut by randomly oriented planes[2]
- The smaller cut parts become the binder, the rest remains the WC
- Parameters:
  (1) number of cuts
  (2) binder volume fraction

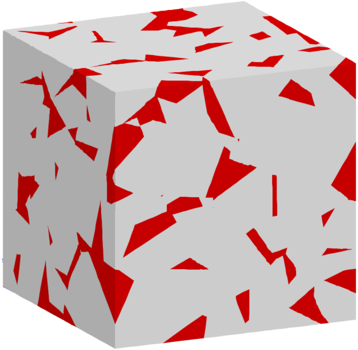

Binder phase

[1] Chris Rycroft `math.lbl.gov/voro++/`

[2] Tkalich, Yastrebov, Cailletaud, Kane, *Int J Solids Struct* 128 (2017)

Microstructural mechanical model: 3D

Microstructural model

- Generate Voronoi tesselation (voro++[1])
- Every Voronoi grain is cut by randomly oriented planes[2]
- The smaller cut parts become the binder, the rest remains the WC
- Parameters:
  (1) number of cuts
  (2) binder volume fraction

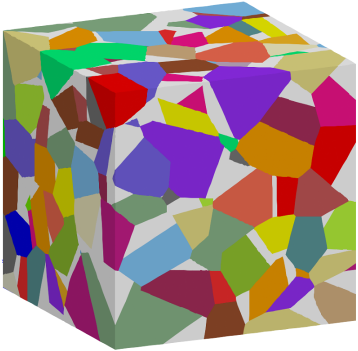

WC grains

[1] Chris Rycroft `math.lbl.gov/voro++/`

[2] Tkalich, Yastrebov, Cailletaud, Kane, *Int J Solids Struct* 128 (2017)

Microstructural mechanical model: 3D

Microstructural model

- Generate Voronoi tesselation (voro++[1])
- Every Voronoi grain is cut by randomly oriented planes[2]
- The smaller cut parts become the binder, the rest remains the WC
- Parameters:
  (1) number of cuts
  (2) binder volume fraction

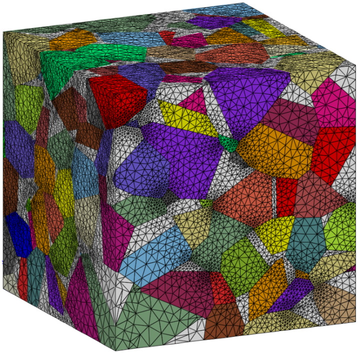

Finite element mesh

[1] Chris Rycroft `math.lbl.gov/voro++/`

[2] Tkalich, Yastrebov, Cailletaud, Kane, *Int J Solids Struct* 128 (2017)

Microstructural mechanical model: 3D examples

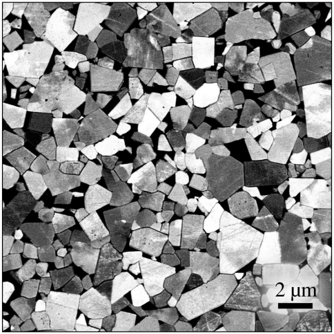

WC/Co microstructure (SEM)

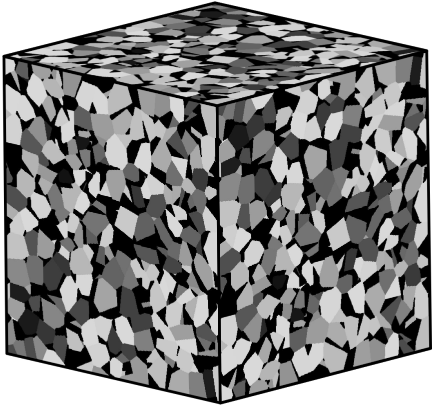

WC/Co artificial microstructure

2 500 grains

Microstructural mechanical model: 3D examples

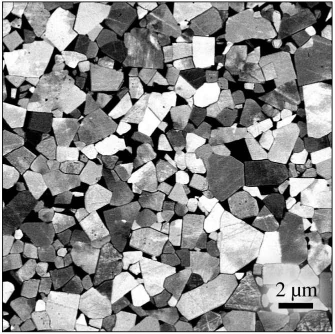

WC/Co microstructure (SEM)

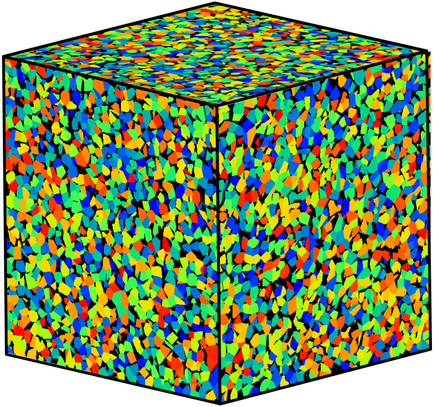

WC/Co artificial microstructure

30 000 grains

Mean-field model

- Notations: $\underline{\underline{E}} = \langle \underline{\underline{\varepsilon}} \rangle$, $\underline{\underline{\Sigma}} = \langle \underline{\underline{\sigma}} \rangle$ with $\langle \bullet \rangle = \frac{1}{V} \int_V \bullet \, dV$
- Effective elastic tensor $\underset{\sim}{C}_{\text{eff}}$
- Strain decomposition: global $\underline{\underline{E}} = \underset{\sim}{C}_{\text{eff}}^{-1} : \underline{\underline{\Sigma}} + \underline{\underline{E}}^p$, local $\underline{\underline{\varepsilon}}_i = \underset{\sim}{C}_i^{-1} : \underline{\underline{\sigma}}_i + \underline{\underline{\varepsilon}}_i^p$
- Eshelby tensor[1] $\underset{\sim}{S} = \dfrac{1}{15(1-\nu_{\text{eff}})} \left[(5\nu_{\text{eff}} - 1) \underline{\underline{I}} \otimes \underline{\underline{I}} + 2(4 - 5\nu_{\text{eff}}) \underset{\sim}{I} \right]$

  with $\underline{\underline{I}} \sim \delta_i^j$, $\underset{\sim}{I} \sim \frac{1}{2}(\delta_i^k \delta_j^l + \delta_i^l \delta_j^k)$
- Iterative procedure to identify the effective elastic tensor[2]

$$\underset{\sim}{C}_{\text{eff}}^{k+1} = \sum_i f_i \underset{\sim}{C}_i : \left[\underset{\sim}{I} + \underset{\sim}{S}^k : \left(\underset{\sim}{C}_{\text{eff}}^{-1} : \underset{\sim}{C}_i - \underset{\sim}{I} \right) \right]^{-1}$$

- Stress in phases: $\underline{\underline{\sigma}}_i = \underset{\sim}{A}_i : \underline{\underline{\Sigma}} + \underset{\sim}{A}_i : \underset{\sim}{C}^* : (\underline{\underline{\beta}} - \underline{\underline{\beta}}_i)$ with

$$\underset{\sim}{C}^* = \underset{\sim}{C}_{\text{eff}} : (\underset{\sim}{I} - \underset{\sim}{S}) \text{ and } \underset{\sim}{A}_i = \left[\underset{\sim}{S} + \underset{\sim}{C}^* : \underset{\sim}{C}_i^{-1} \right]^{-1}$$

- Accommodation tensors[3,4] $\underline{\underline{\beta}}_i$ with evolution

$$\dot{\underline{\underline{\beta}}}_i = \dot{\underline{\underline{\varepsilon}}}_i^p - \|\dot{\underline{\underline{\varepsilon}}}_i^p\| \left(D_i^s \underline{\underline{\beta}}_i^{sp} \underline{\underline{I}} + D_i^{dev} \underline{\underline{\beta}}_i^{dev} \right)$$

[1] Eshelby. *Proc Royal Soc L: A* 241 (1957)
[2] Kröner. *J Mech Phys Solids* 25 (1977)
[3] Cailletaud, Pilvin. *Rev Eur Elem Fin* 3 (1994)
[4] Cailletaud, Coudon. Ch. in *Scale Transition Rules Applied to Crystal Plasticity* (2015)

Mean-field model

- Notations: $\underline{\underline{E}} = \langle \underline{\underline{\varepsilon}} \rangle$, $\underline{\underline{\Sigma}} = \langle \underline{\underline{\sigma}} \rangle$ with $\langle \bullet \rangle = \frac{1}{V} \int_V \bullet \, dV$
- Effective elastic tensor $\underset{\sim}{C}_{\text{eff}}$
- Strain decomposition: global $\underline{\underline{E}} = \underset{\sim}{C}_{\text{eff}}^{-1} : \underline{\underline{\Sigma}} + \underline{\underline{E}}^p$, local $\underline{\underline{\varepsilon}}_i = \underset{\sim}{C}_i^{-1} : \underline{\underline{\sigma}}_i + \underline{\underline{\varepsilon}}_i^p$
- Eshelby tensor[1] $\underset{\sim}{S} = \frac{1}{15(1-\nu_{\text{eff}})} \left[(5\nu_{\text{eff}} - 1) \underline{\underline{I}} \otimes \underline{\underline{I}} + 2(4 - 5\nu_{\text{eff}}) \underset{\sim}{I} \right]$

  with $\underline{\underline{I}} \sim \delta_i^j$, $\underset{\sim}{I} \sim \frac{1}{2}(\delta_i^k \delta_j^l + \delta_i^l \delta_j^k)$
- Iterative procedure to identify the effective elastic tensor[2]

$$\underset{\sim}{C}_{\text{eff}}^{k+1} = \sum_i f_i \underset{\sim}{C}_i : \left[\underset{\sim}{I} + \underset{\sim}{S}^k : \left(\underset{\sim}{C}_{\text{eff}}^{-1} : \underset{\sim}{C}_i - \underset{\sim}{I} \right) \right]^{-1}$$

- Stress in phases: $\underline{\underline{\sigma}}_i = \underset{\sim}{A}_i : \underline{\underline{\Sigma}} + \underset{\sim}{A}_i : \underset{\sim}{C}^* : (\underline{\underline{\beta}} - \underline{\underline{\beta}}_i)$ with

  $\underset{\sim}{C}^* = \underset{\sim}{C}_{\text{eff}} : (\underset{\sim}{I} - \underset{\sim}{S})$ and $\underset{\sim}{A}_i = \left[\underset{\sim}{S} + \underset{\sim}{C}^* : \underset{\sim}{C}_i^{-1} \right]^{-1}$
- Accommodation tensors[3,4] $\underline{\underline{\beta}}_i$ with evolution

$$\dot{\underline{\underline{\beta}}}_i = \dot{\underline{\underline{\varepsilon}}}_i^p - \|\dot{\underline{\underline{\varepsilon}}}_i^p\| \left(D_i^s \beta_i^{sp} \underline{\underline{I}} + D_i^{dev} \underline{\underline{\beta}}_i^{dev} \right)$$ - for each phase (WC and binder)

[1] Eshelby. *Proc Royal Soc L: A* 241 (1957)
[2] Kröner. *J Mech Phys Solids* 25 (1977)
[3] Cailletaud, Pilvin. *Rev Eur Elem Fin* 3 (1994)
[4] Cailletaud, Coudon. Ch. in *Scale Transition Rules Applied to Crystal Plasticity* (2015)

3D results

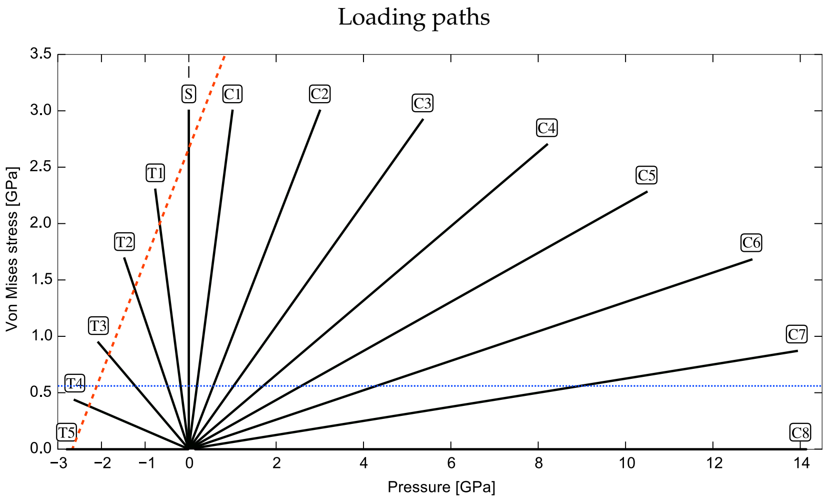

Loading paths
Von Mises stress [GPa]
Pressure [GPa]
3.5
3.0
2.5
2.0
1.5
1.0
0.5
0.0
−3
−2
−1
0
2
4
6
8
10
12
14
S
C1
C2
C3
C4
C5
C6
C7
C8
T1
T2
T3
T4
T5

3D results

Deformation curves

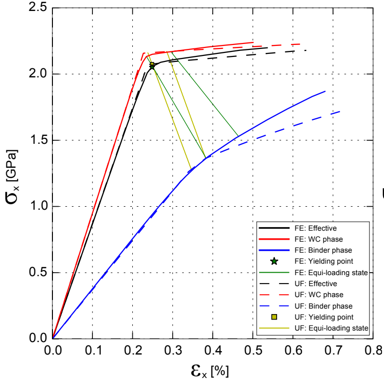

Tensile (T2) loading

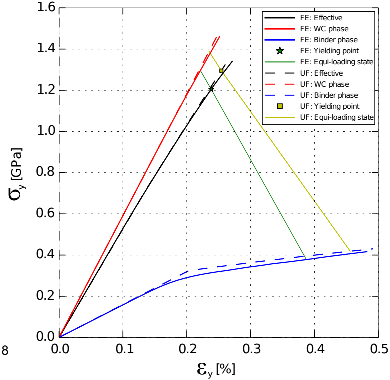

Shear (S) loading

Elastic limit is determined at the point when the plastic strain $p > 0.01$ %,

where $p = \sqrt{\frac{2}{3}\underline{\underline{E}}^p : \underline{\underline{E}}^p}$ and $\underline{\underline{E}}^p = \underline{\underline{E}} - \underline{\underline{C}}_{\text{eff}} : \underline{\underline{\Sigma}}$

3D results

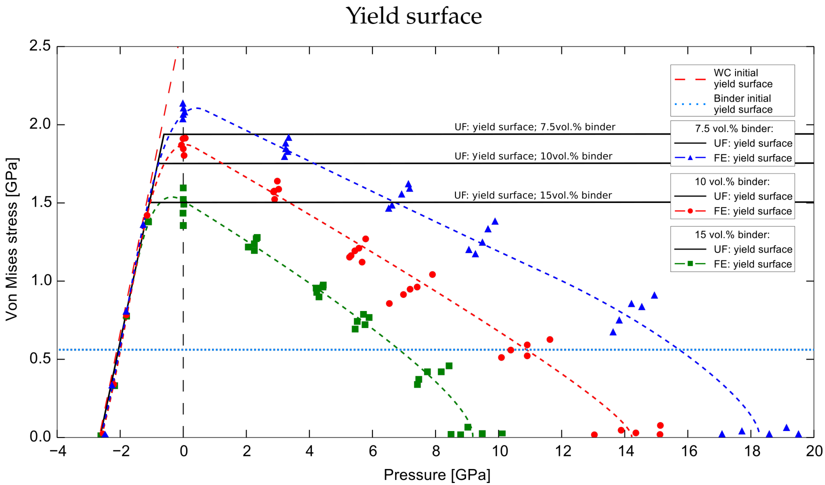

Elastic limit is determined at the point when the plastic strain $p > 0.01$ %,

where $p = \sqrt{\frac{2}{3}\underline{\underline{E}}^p : \underline{\underline{E}}^p}$ and $\underline{\underline{E}}^p = \underline{\underline{E}} - \underline{\underline{C}}_{\text{eff}} : \underline{\underline{\Sigma}}$

Simulation of the tool-rock interaction

- Quasi-static FEA
- Elastic rock cylinder $E = 79$ GPa, $\nu = 0.26$ (Kuru granite[1])
- Frictional (lubricated) contact $\mu = 0.3$
- Oblique impacts at different angles
- Every Gauss point integrates the calibrated mean-field β-model

[1] Hokka et al, *Int J Impact Eng* 91 (2016)

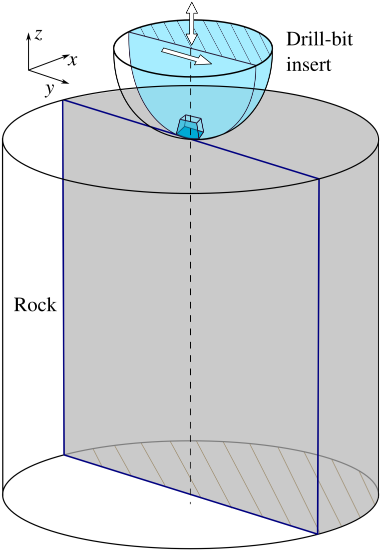

Simulation of the tool-rock interaction

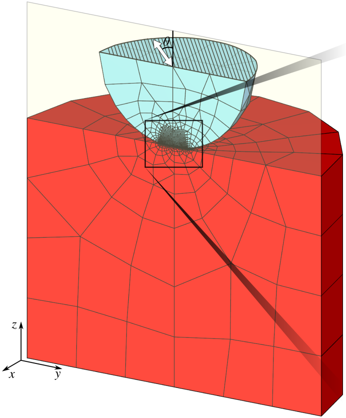

(a)

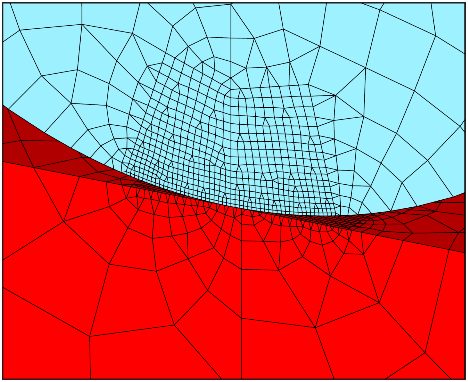

(b)

Macro-scale results

Normal impact

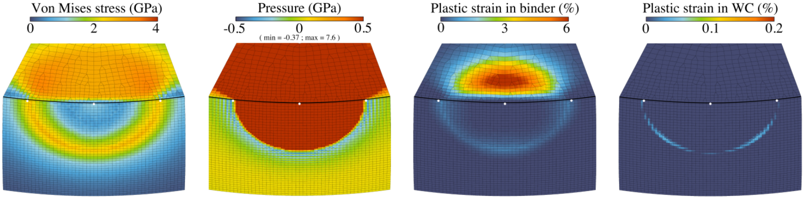

Oblique impact at $\varphi = \pi/12$

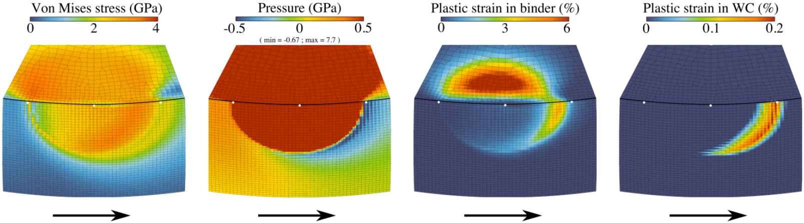

Direction of motion

Representative loading paths $\sigma_{ij}(t)$

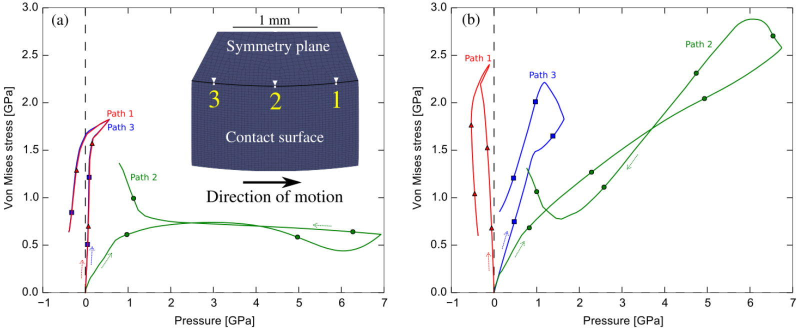

Normal impact

Oblique impact at $\varphi = \pi/12$

Point 2.

Joint probability density of microstress state in σ_{vM}–P space.

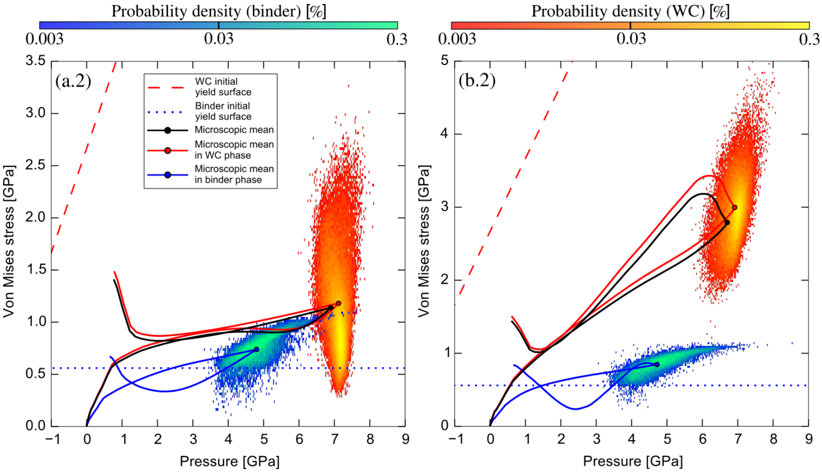

Normal impact

Oblique impact at $\varphi = \pi/12$

Point 1.

Joint probability density of microstress state in σ_{vM}–P space.

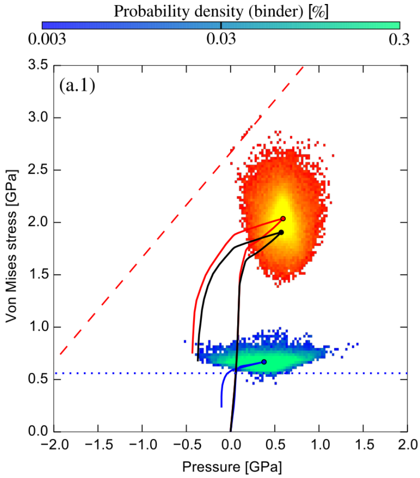

Normal impact

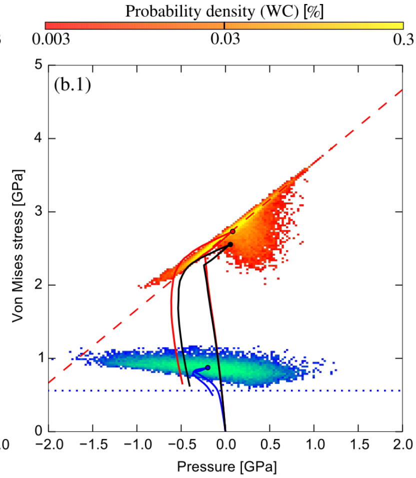

Oblique impact at $\varphi = \pi/12$

Point 2.

Accumulated plastic strain in the binder and WC

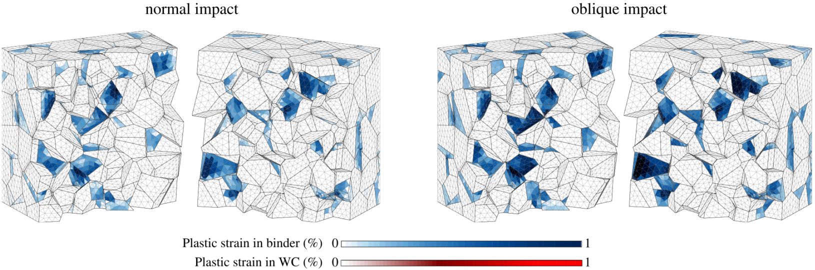

Micro-scale results 2

Point 1.

Accumulated plastic strain in the binder and WC

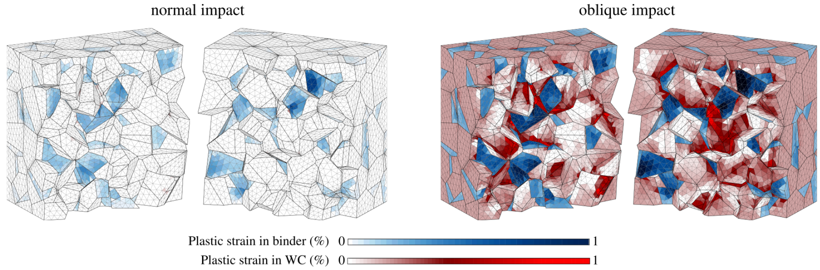

Wear at drill bit inserts

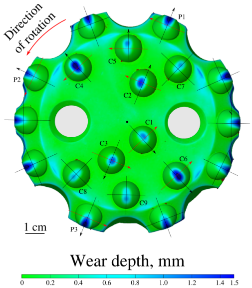

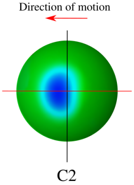

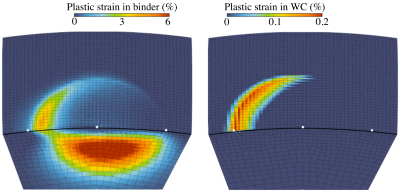

Wear at drill bit inserts

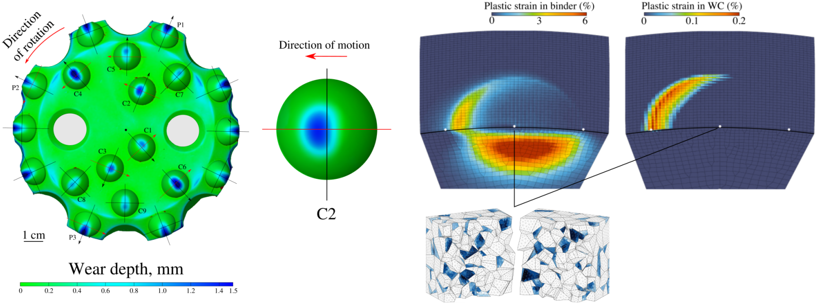

Wear at drill bit inserts

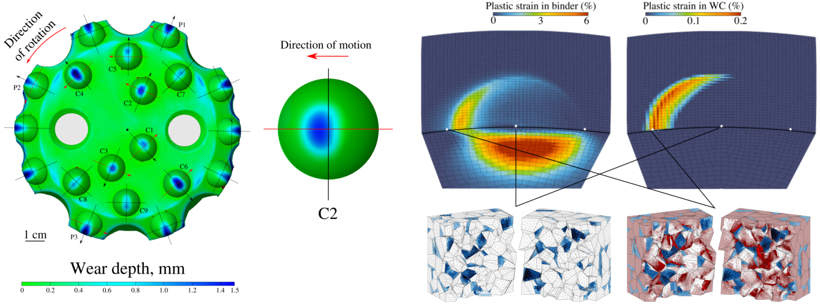

Conclusion: recall of methodology

Micro

1. Construct FE RVE
2. FE RVE: proportional loadings
3. Calibration of the mean field β-model

Macro

4. FE structural simulation with the embedded β-model
5. Extract near-surface representative loading paths

Micro

6. FE RVE: representative loadings

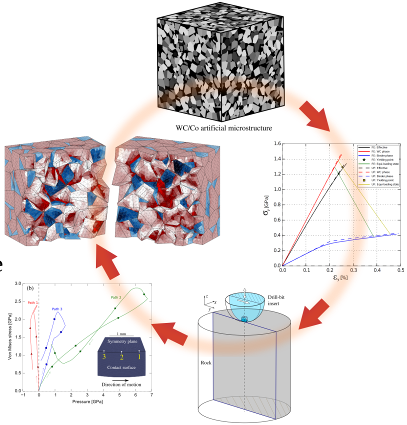

- WC grain anisotropy
- Residual stresses due to sintering[1]
- Binder's loose due to melting (coupled thermo-mechanical model)
- Bore-hole's floor topography
- WC/WC decohesion

[1] Krawitz, Reichel, Hitterman. *Mater Sci Eng* A119 (1989)

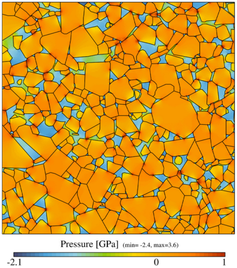

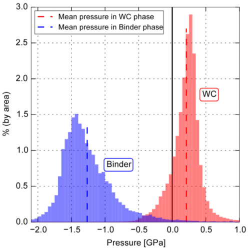

2.5D microstructure
Spatial and probability distribution of pressure after sintering from 800 to 20 °C.

Perspectives

- WC grain anisotropy
- Residual stresses due to sintering[1]
- Binder's loose due to melting (coupled thermo-mechanical model)
- Bore-hole's floor topography
- WC/WC decohesion

[1] Krawitz, Reichel, Hitterman. *Mater Sci Eng* A119 (1989)

Biaxial compression

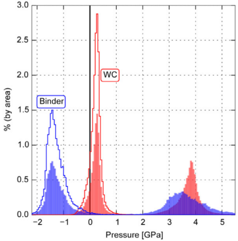

Pure shear

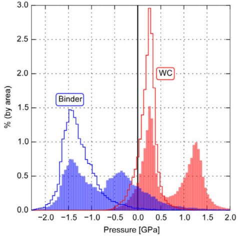

2.5D microstructure
Probability distribution after subsequent loading

Perspectives

- WC grain anisotropy
- Residual stresses due to sintering[1]
- Binder's loose due to melting (coupled thermo-mechanical model)
- Bore-hole's floor topography
- WC/WC decohesion

[1] Krawitz, Reichel, Hitterman. *Mater Sci Eng* A119 (1989)

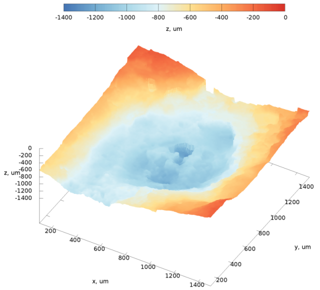

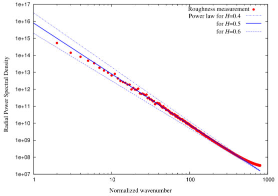

Crater in Kuru granite after a single impact[2]

[2] Tkalich et al, Wear 386-387 (2017)

Perspectives

- WC grain anisotropy
- Residual stresses due to sintering[1]
- Binder's loose due to melting (coupled thermo-mechanical model)
- Bore-hole's floor topography
- WC/WC decohesion

[1] Krawitz, Reichel, Hitterman. *Mater Sci Eng* A119 (1989)

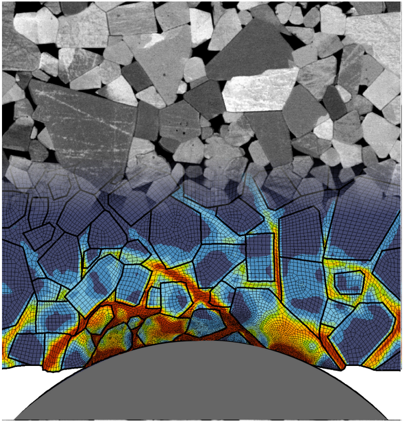

Rigid rock asperity impacting WC hardmetal

Perspectives

- WC grain anisotropy
- Residual stresses due to sintering[1]
- Binder's loose due to melting (coupled thermo-mechanical model)
- Bore-hole's floor topography
- WC/WC decohesion

[1] Krawitz, Reichel, Hitterman. *Mater Sci Eng* A119 (1989)

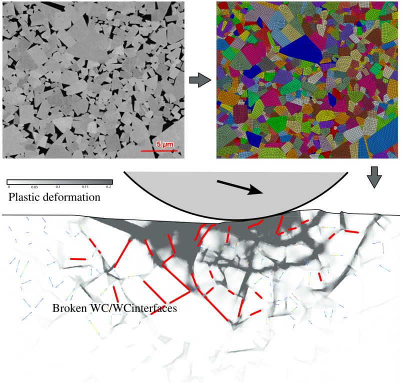

2D simulation of oblique rock asperity impact of WC hardmetal microstructure
Account for the effect of weak WC/WC interfaces (cohezive zone model)

Thank you for you attention!

Dmitry Tkalich[★▲], Vladislav A. Yastrebov[★]
Alexandre Kane[•], Georges Cailletaud[★]

[★] *MINES ParisTech, Centre des Matériaux, CNRS UMR, Evry, France*

[▲] *National University of Singapore, Singapore*
[•] *Sintef, Trondheim, Norway*

@ CMCS, Paris, France
November 8, 2017